

Improved Nonlinear Model Implementation for VCSEL Behavioral Modeling in Radio-Over-Fiber links

Andrea Giovannini, Muhammad Usman Hadi, Lucas Iogna Prat, Najett Neji, Zerihun Gedeb Tegegne, Carlos Viana, Anne-Laure Billabert, Jean-Marc Laheurte, Jacopo Nanni, Diego Masotti, Giovanni Tartarini and Jean-Luc Polleux

Abstract— This paper proposes an improved model for the nonlinear behavior of the components of Radio-over-Fiber (RoF) links focusing here on the laser source. In a previous work, it was shown with a flexible new opto-microwave design approach a first behavioral model of RoF links that exploited the hyperbolic tangent function (the so-called *tanh* model) to model the high-power nonlinearities. Since this was not sufficient to simulate adequately all the nonlinearities, in this work, for the first time in the authors' knowledge, the improved nonlinear model based on Cann's model is developed, on an electro optic transducer. Then the amplitude-to-amplitude conversion of the link is better taken into account with the introducing of nonlinear properties of the link at high input power in the model. The new transfer equation includes several parameters that can be adjusted to adapt the model to any of the components, especially the photo-emitters under study, which are the main cause of this type of nonlinear behavior of the system. In particular, this improved model is applied on the state-of-the-art 850 nm GaAs Vertical Cavity Surface Emitting Laser (VCSEL), simulating several Figures of Merit such as the Error-Vector Magnitude (EVM) of a Long Term Evolution (LTE) signal with a Quadrature Phase Shift Keying (QPSK) and the output amplitude-modulated power versus input amplitude-modulated power, also called AM/AM curve. This new proposed nonlinear model outperforms other existing behavioral models and its non linear simulation better fits with the measurements. Finally, we conclude that the performance improvement highly depends on the nonlinearity sharpness parameter, depending on the frequency and the bias current.

Index Terms—Behavioral model, Radio-over-Fiber (RoF), Vertical cavity surface emitting laser (VCSEL), Microwave-Photonics, improved Cann's nonlinear model.

I. INTRODUCTION

As a consequence of the increasing demand of high-speed and broadband wireless access, a trend of developing

Radio-over-Fiber (RoF) technologies has appeared as a solution to reduce the infrastructure costs [1]–[5]. Indeed, at very high frequencies, the coverage distance is limited up to several meters due to the substantial signal attenuation in these frequency bands. Hence, radio-over-fiber (RoF) technologies are a good alternative to improve the coverage of Home Area Networks (HAN) [6] and can be privileged in a larger scale of applications as in stadium or tunnel.

To fulfill application requirements, complex modulation schemes are transmitted through an optical source into the fiber and re-emitted after optical detection into the final radio-cell. It is therefore important to preserve the quality of the radio signal through the RoF link and to properly design it in terms of frequency, noise and non-linearity behavior.

Behavioral modeling is in this regard an important approach that helps to provide a simple analysis of the component behavior, laser or photodetector for instance, into a system, or vice-versa to determine what are the minimum requirements for the device to operate into a given system. They opposed themselves to compact-circuit models or rate equations models [7] which requires a precise knowledge of the device physics. As part of behavioral models, we distinguished those models based on pure analytical equations such as Volterra series or memory polynomial such as those applied to lasers in [8] and [9] and those based on analytical equations to represent the system metrics of the device. We focus our interest on the latter behavioral models category that refers to the figures of merit of the device that provide a more flexible approach.

Many approaches to develop figures of merit taking into account the optical devices characteristics have been proposed in [1]–[22]. In [6], a complete set of Opto-Microwave (OM) quantities has been identified, which connects optical devices

This work was partly supported by the French FUI8 ORIGIN project and FUI MORF project and by the Università Franco Italiana - Università Italo Francese, through the sponsorship of the Joint Doctorate Project C3-2025 Efficient Wireless Coverage of In-Building Environments with Low Electromagnetic Impact within the Call Vinci 2019. (*Corresponding author: Andrea Giovannini.*)

Andrea Giovannini, Jacopo Nanni, Diego Masotti, Muhammad Usman Hadi and Giovanni Tartarini are with the Dipartimento di Ingegneria dell'Energia Elettrica e dell'Informazione "Guglielmo Marconi", Università di Bologna, 40136 Bologna (BO), Italy (e-mail: andrea.giovannini14@unibo.it; jacopo.nanni3@unibo.it; diego.masotti@unibo.it; usmanhadi@ieee.org; giovanni.tartarini@unibo.it).

Anne-Laure Billabert is with Le Cnam, ESYCOM-CNRS, 75003 Paris, France (e-mail: anne-laure.billabert@lecnam.net).

Jean-Luc Polleux, Jean-Marc Laheurte, Lucas Iogna Prat, Zerihun Gedeb Tegegne are with Univ Gustave Eiffel, CNRS, ESYCOM, F-77454 Marne-la-Vallée, France (e-mail: jean-luc.polleux@esiee.fr; jean-marc.laheurte@univ-eiffel.fr; ip_lucas@hotmail.com; ztzerihun0@gmail.com).

Najett Neji is with Université Paris Saclay, Univ Evry, 91025 Evry (e-mail: najett.neji@univ-evry.fr).

Carlos Viana is with ICON Photonics, SAS, France (e-mail: carlos.viana@icon-photonics.com).

with microwave tools and concepts. These figures of merit, namely Opto-Microwave power, gain, noise figure, compression point (OM- P_{1dB}) and third-harmonic intermodulation product (OM- IP_3) have been defined, and behavioral models were proposed for the laser, the fiber and the photodetector. These models were implemented in a standard microwave systems simulator named ADS software from Keysight Technologies and efficiently represented the noise figure and the non-linearity of the link. However, some deviations to the measured non-linearity of the laser were observed [6].

In addition, several models have been developed in the last decades to describe the RoF links behavior [23] [24]. Due to the similarities between the large signal behavior of both lasers (e.g. VCSEL LIV curves [25] [27]) and power amplifiers (e.g. amplifier transfer function), some models have been developed, based on the existing literature about behavioral modeling of power amplifiers [27]-[35]. In [6], the large signal behavior is modeled by using the Hyperbolic Tangent (tanh) to fit the simulations with the measurements; an approach that was already proposed in the early 1990s. However, the main disadvantage of this method is that this function does not allow the user to adapt the model to any kind of device by changing the knee sharpness of the amplitude-to-amplitude (AM/AM) curve. In 1980 [36], Cann proposed an instantaneous nonlinearity model (in the context of radio-frequency power amplifiers) with adjustable knee sharpness; however, this model led to non-consistent results for two-tone intermodulation test, because of its nonanalyticity at zero. In 2012 [37], Cann proposed an improved nonlinearity model in order to overcome the pointed issues. Hence, in this paper, we adapt the Cann non-linear models of the RF power amplifiers [36] to photonic subsystems (such as lasers, but also photodetectors, and photonic link) as an improved solution for the behavioral model of RoF links.

The paper is organized as follows. In Section II, the RoF link system as well as the experimental setup for its characterization is described. In Section III, the behavioral modeling is developed. First a description of the hyperbolic tangent model is proposed. The Cann's non-linearity behavior model is then proposed and adapted to RoF non-linear model. In Section IV, we present the complete opto-microwave model and we analyze its comparison to measurements including EVM for LTE signals transmission. Finally, in Section V, we summarize the main contributions and further work.

II. RoF LINK DESCRIPTION AND EXPERIMENTAL SETUP

The concept of Radio-over-Fiber directly modulates the laser with an RF signal, transmits the modulated optical signal through the fiber, and detects its RF envelope through a photodetector. As described in [6], this scheme is suitable for home area networks (HAN) and enables the use of low-cost opto-electronic components such as Vertical Cavity Emitting Surface Lasers (VCSEL) together with multimode fiber, even up to millimeter-wave frequencies when using Intermediate-Frequency (IF) scheme. This paper however refers to a Direct-

RoF scheme where the RF signal is within the bandwidth of the VCSEL and directly modulates the laser. This constitutes the core of both Direct and IF RoF systems.

The typical architecture of the RoF link composed of a laser, an optical fiber and a photodetector is shown in figure 1.

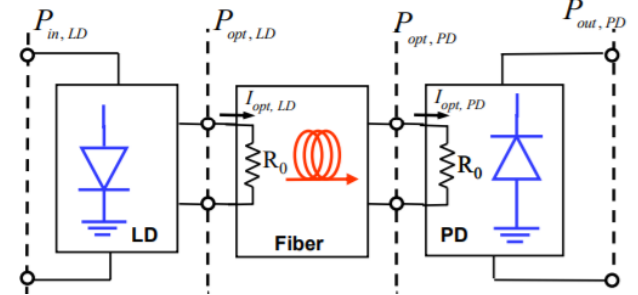


Fig. 1. RoF link architecture.

For this study, the link is composed by a VCSEL laser, a single mode optical fiber connected to a variable optical attenuator and an InGaAs-based high speed photodiode (1414-50 New Focus). The laser is a 10 GHz GaAs VCSEL die, under probe, operating at 850 nm from Philips Technologies ULM Photonics GmbH. The purpose of the variable optical attenuator is to keep the fiber's attenuation at a constant level, in order to easily compare the measurements at different biasing conditions. In particular, this total attenuation is set to be 5 dB.

The laser's optical aperture diameter is 8 μm and the technology is based on mesa etching and subsequently laterally oxidized current apertures [32]-[35]. The die is biased through a 100 μm pitch RF GSG probe. The laser output beam is coupled to a lensed multimode fiber probe whose position is precisely fixed above the die with a nanopositioner to optimize the coupling efficiency. The photodetector is used as a reference photodetector for the extraction of the VCSEL performance. It is highly linear and shows a flat frequency response up to 25 GHz, with a responsivity of 0.22 A/W at 850nm, under short-circuit conditions.

The optical fiber presents a defined angle of 6° with respect to the orthogonal direction of the VCSEL die in order to avoid parasitic optical cavities into the laser, due to backscattered light. The fiber output extremity is connected to the photoreceiver. The output signal is then connected to an Electrical Spectrum Analyzer (ESA).

TABLE I
LD AND PD SPECIFICATIONS FOR OUR TEST BENCH

Parameter	VCSEL LD	New Focus PD	Units
IP_{1dB}	6	15	dBm
Gain	-27	-19	dB
Wavelength	850	850	nm
RIN	-147.5	-	dB/Hz
f_{-3dB}	12.3	25	GHz

The characteristics of the VCSEL laser and the New Focus photodiode used for the experimental measurements are

summarized in Table I, where IP_{1dB} is the input 1 dB compression point, RIN is the Relative Intensity Noise of the laser, and f_{-3dB} is the cut-off frequency.

III. BEHAVIORAL MODELLING OF ROF LINK

A. Tanh model

In our previous work [6], the input-output characteristics of both laser and photodetector were modelled by using the hyperbolic tangent as the transfer function to fit the simulations with the measurements. In that case, the definition of the equivalent optical current was given in (1):

$$I_{out} = I_s \cdot \tanh\left(\frac{G \cdot I_{in}}{I_s}\right) \quad (1)$$

Where I_{out} is the component's output current, i.e. in our case the equivalent optical current at the laser's output $I_{opt,LD}$ as defined later in (2), I_s is the limit value of the output signal which provides the saturation effect, G is the opto-microwave gain in the linear region, and I_{in} is the injected input current to the component, i.e. the electrical injection current of the laser. In addition, $I_{opt,LD}$ is given by (2):

$$I_{opt,LD} = \alpha_c P_{opt,LD} \quad (2)$$

Where α_c is the conversion coefficient of the optical power to electrical current (considered equal to 1 A/W in our study). The opto-microwave (OM) gain of the laser, denoted G_{LD}^{OM} , is expressed as the ratio of the laser's equivalent OM output power to the electrical power at its input. When considering a 50 Ohm laser, the laser OM gain is expressed by (3):

$$G_{LD}^{OM} = \frac{P_{opt,LD}}{P_{in,LD}} = S_{LD}^2 \quad (3)$$

Where S_{LD} is the laser's slope efficiency. Similarly, the OM gain of the photodiode, denoted G_{PD}^{OM} , is expressed as the ratio of the output electrical power provided by the photodiode to the equivalent OM power delivered to its input. When considering a matched photodiode, it is given by:

$$G_{PD}^{OM} = \frac{P_{out,PD}}{P_{opt,PD}} = R_{PD}^2 \quad (4)$$

Where R_{PD} is the photodiode's responsivity. This model allows to control the output saturation level and the slope of the curve by changing the parameters I_s and G respectively. However, it is not possible to control the sharpness of the knee. For this reason, it was imperative to find a new model capable of simulating this behavior.

B. First Cann's nonlinear model and its limit

In [36], Cann proposed an instantaneous nonlinear model for power amplifiers to analyze their non-linearity focusing on a variable named "knee sharpness". This model was based on the frequency response of a RC high pass filter, that better implements the desired shape of the equivalent output optical current versus input current.

Equation (5) shows the Cann's first non-linear model, where y represents the equivalent output optical current, L is the output limit level, x is the input current and s is the knee sharpness variable.

$$y(x) = \frac{L}{\left(1 + \left(\frac{L}{x}\right)^s\right)^{1/s}} \quad (5)$$

This model is efficient for many reasons. First, it has a linear behavior for small input signals, and it tends to an asymptotic defined limit level for large input signals. In addition, it is an economical model to compute (closed form and analytic), capable of modeling various knee sharpness values by changing a single parameter. However, this model gives incorrect results for the third-order intermodulation product (IP_3), since it has a nonphysical behavior for the large input signal regime. Because of the nonphysical behavior, the Cann model gives imprecise predictions for nonlinear products [37].

C. Improved Cann's nonlinear model

In 2012, Cann developed an improved model where the limitations of its first nonlinear model were solved [37]. The solution for the equivalent optical current in this model is given by (6), where the variables in this equation can be related to our RoF system. Hence, y represents the output equivalent optical current of the laser, x is the input current of the laser, g is a gain parameter well approximated by the slope efficiency of the laser for sufficiently high k , L is the output limit level (saturation level) and k is the sharpness parameter.

$$y(x) = \frac{L}{k} \ln \left(\frac{1 + e^{k(\frac{gx}{L} + 1)}}{1 + e^{k(\frac{gx}{L} - 1)}} \right) - L \quad (6)$$

Cann demonstrated that this model suitably behaves for two-tone intermodulation products [37], and this outperforms his first model. While the other parameters of the model (i.e. gain and saturation level) can be easily measured, the sharpness parameter k is apparently determinable only with heuristics. A deeper analysis of the model allows to relate the parameter k to the input IP_3 (IIP_3) and the input P_{1dB} (IP_{1dB}). In fact, as mentioned before, the gain parameter g in (6) is formerly not exactly equal to the slope efficiency of the laser, but is linked to it through (7):

$$g = \frac{1 + \cosh(k)}{\sinh(k)} S_{LD} \quad (7)$$

This relation is obtained by considering that the current linear gain (i.e. $\sqrt{G_{LD}^{OM}}$) must be equal to the first derivative of (6) computed in 0. The multiplying factor depends only on k and tends to 1 for increasing values of k . If $k > 3$ then $g > 0.9 S_{LD}$, so for k sufficiently high $g = S_{LD}$ is a good approximation. If we derivate up to the 3rd order and consider the IP_3 condition, then the saturation level L is linked to the IIP_3 through

$$L = kg \sqrt{\frac{3}{2} \cdot \frac{IIP_3}{1 + \cosh(k)}} \quad (8)$$

This last relation can be used to determine k and it requires to measure the saturation current of the laser. An alternative is to consider the P_{1dB} condition in order to obtain a relation dependent only on k . Assuming that in the P_{1dB} biasing point the power associated to non-linear harmonics is negligible, then the following relation is found:

$$\left[\ln \left(\frac{1 + e^{\sqrt{\frac{4IP_{1dB}}{3IP_3}(1+\cosh(k))+k}}}{1 + e^{\sqrt{\frac{4IP_{1dB}}{3IP_3}(1+\cosh(k))-k}}} \right) - k \right] = \sqrt{\frac{4}{3(1 - \cosh(k))} \frac{IP_{1dB}}{IP_3}} 10^{-1/20} \quad (9)$$

Equation (9) finally depends only on k and on the ratio between IP_{1dB} and IIP_3 . Isolating k from (9) is rather challenging, but through numerical interpolation it is possible to find an appropriate polynomial approximating the curve. The Cann's model has been validated on commercial electrical amplifier and soft clipping limiters. Owing to this result, the choice has been done to exploit this Cann model to model an electro-optic transducer with a behavior approach. The steps and results are presented in the next paragraph.

D. Electro-optic modelling based on Cann's model

The Cann's improved model is then introduced into the RoF model developed in [6] using the microwave circuit and system Keysight Technologies simulation software. The laser, the optical fiber and the photodetector were implemented through the use of Symbolically Defined Devices (SDD), which was introduced in its respective internal blocks. In each SDD cell, we define the transfer function of our model (only for the laser and photodetector since the optical fiber is considered as a linear system).

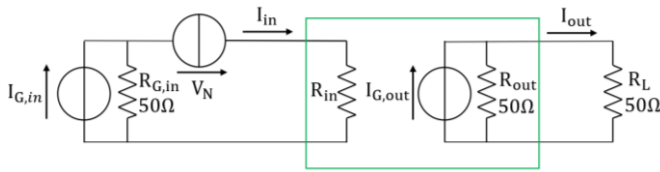


Fig. 2. Laser (green box) internal model.

The laser model is implemented following the equivalent scheme in figure 2. A current generator with an internal 50 Ω resistance $R_{G,in}$ provides a current $I_{G,in}$ to the circuit. The noise sources of the laser are implemented into the laser model through a noise voltage source V_N in $\mu V/\sqrt{Hz}$ describing the RIN. The RIN function is implemented using the conventional frequency response given in [38] and using equation (10).

$$RIN(f) = A \cdot \frac{4\pi^2 \cdot f^2 + B}{16\pi^4(f_R^2 - f^2)^2 + 4\pi^2 \cdot \gamma^2 \cdot f^2} \quad (10)$$

Where A and B are device-dependent constants, f is the

modulation frequency, f_R is the relaxation oscillation frequency and γ the damping factor of the intrinsic laser.

I_{in} is the laser injection current while R_{in} is the input resistance of the laser, which can be conveniently mismatched with respect to the generator if a reflection needs to be taken into account. However, in this work we assume a matched input port. On the output side, a generator with an internal 50 Ω resistance $R_{G,out}$ provides a current $I_{G,out}$ based on (6) and implementing also a frequency dependent equation and non-linear analytical equation according to [23]. The output of the device I_{out} represents the output optical power, $P_{opt,LD}$, as an equivalent electrical current noted $I_{opt,LD}$ feeding a matched 50 Ω load R_L (in this case it corresponds to the input impedance of the optical fiber OM block). The laser overall modulation frequency response $H(f)$ is implemented through a common third order system, given by equation (11):

$$H(f) = \frac{1}{1 + j \cdot \frac{f}{f_p}} \cdot \frac{f_R^2}{f_R^2 - f^2 + j \cdot f \cdot \frac{\gamma}{2\pi}} \quad (11)$$

Where f_p is the electrical parasitic cutoff frequency due to the access lines. The large signal behavior is then implemented into the model by introducing the modified Cann model equation (6), where y is the output current $I_{opt,LD}$ of the laser, x is the injected input current into the laser active part, and g is the small-signal responsivity divided by 1A/W to suit the conversion $P_{opt,LD}$ to $I_{opt,LD}$. The parameters L , k and g are derivated considering the P_{1dB} and IP_3 as found in (7), (8) and (9). The optical fiber and photodetector model's definitions are described in [6]. The optical fiber model includes the coupling losses between the laser and the fiber. Its attenuation value is slightly adjusted to fit with the measurements, as misalignments may vary. Considering the short length of the fiber, the frequency dependent term of the attenuation due to modal dispersion has not been considered. This device is considered linear and noiseless. The P_{1dB} value of the photodiode model is set to a high value, because the non-linearities of the device are negligible in our case study. To be noted that the model formerly transduces an electrical current into an optical power, represented by the equivalent OM current.

IV. STUDY OF THE RoF LINK: SIMULATIONS WITH THE IMPROVED CANN'S MODEL COMPARED TO RoF MEASUREMENTS

A. System simulation: Gain, AM/AM and EVM curves

By using the previously described model, we investigate several figures of merit (OM gain, AM/AM curve, and Error Vector Magnitude (EVM) performance) and compare simulation results with measurements. The data of the Gain and the AM/AM curves is relative to the input electrical power of the laser to the output electrical power at the photodiode, with a maximum RF input power of 15 dBm. For this, we perform a measurement of a RoF link that is constituted by the VCSEL laser, multimode optical fiber (MMF) and New Focus photodiode directly modulated at a carrier frequency of 2 GHz.

By knowing the responsivity of the photodiode and the attenuation of the fiber plus the optical attenuator, it is possible to extract the laser's output OM power, useful for the behavioral model. Regarding the EVM measurements, a Long Term Evolution (LTE) signal is transmitted through the RoF link with a Quadrature Phase Shift Keying (QPSK) modulation at a center frequency of 2 GHz and a bandwidth of 20 MHz. A Vector Signal Generator (VSG) Agilent model N5182B MXG X-Series is exploited to generate the signal emulated through a domestic MATLAB code. The VSG-generated signal directly modulates the VCSEL laser. The photo-detected signal is amplified and captured with a Vector Signal Analyser from Rhode&Schwartz. The captured signal is then processed offline in MATLAB and demodulated, followed by EVM estimation.

Fig. 3 presents the comparison of the simulated OM gain (solid lines) with the measured OM gain of the proposed RoF link at 2 GHz where the VCSEL is biased at 8 mA. It can be observed that the simulated curves are fitting with the measurements data.

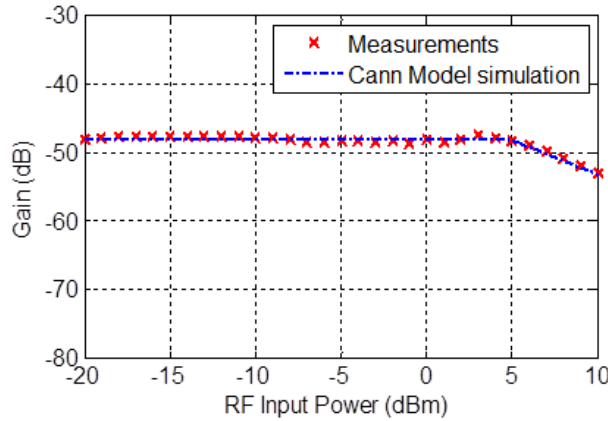


Fig. 3. Measured and simulated opto-microwave gain (at 2 GHz using the VCSEL – 8 mA biasing).

Based on the nonlinear model described above, we also perform the simulations at 2 GHz based on first and improved Cann's nonlinear model as well as tanh model as presented in Fig. 4. It can be noted that the new models are properly fitting with the measurement and behave much better than the tanh model. Indeed, it is impossible to change the shape of the simulated tanh model. Nevertheless, using the improved Cann's model, we can control the shape only by changing the value of the parameter k (see equation (6)).

Now we are interested in the Error Vector Magnitude (EVM) which is an important indicator of the RoF link performance. The measured EVM is compared with respect to the three models (tanh, Cann's and improved Cann's model) as shown in Fig. 5a. The Back-to-Back (B2B) EVM experimental results are also indicated in both figures. In Fig. 5b we can notice that the curve corresponding to the improved Cann model fits better to the measurement data compared to the tanh model especially at high input RF power. Similarly, the improved Cann model fits closer to the experimental data as compared to Cann model itself.

The parameters of the tanh and Cann's models are determined either by measurements or by numerical estimation following a Least Absolute Error (LAE) method, which aims at

minimizing the deviation between the model and the AM/AM measurements. For the estimation of k in the Improved Cann's model (6), we numerically solved (9) and found the values of the ratio IP_{1dB}/IIP_3 for k ranging between 0.1 and 30, then fit the points with a 4th order polynomial. By measuring IP_{1dB} and IIP_3 we then extract k and determine L and g with (7) and (8).

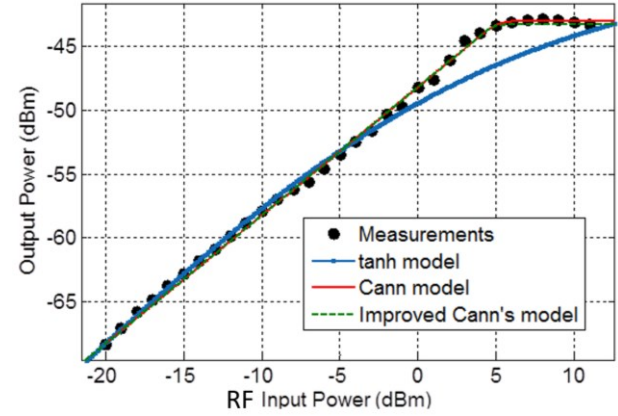


Fig. 4. Measured and simulated AM/AM curves (at 2 GHz using the VCSEL – 8mA DC biasing). The simulation considers first and improved Cann's model as well as tanh model.

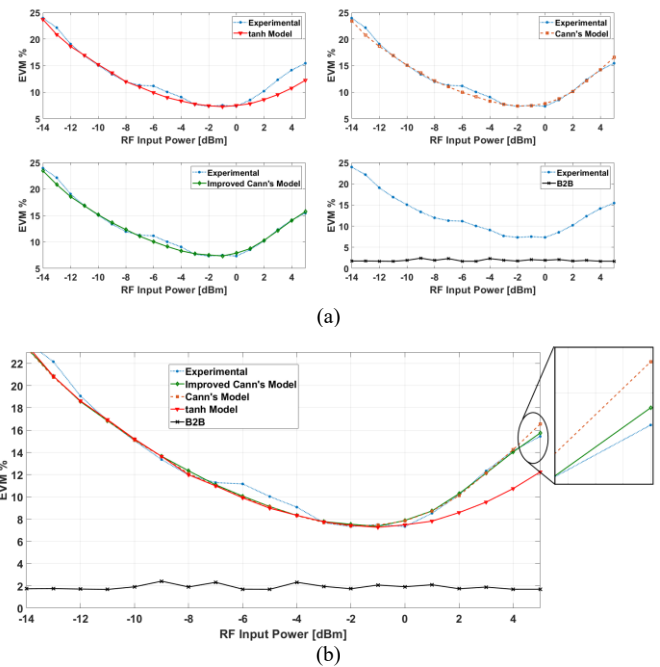


Fig. 5. Measured and simulated EVM curves for the first test bench (at 2 GHz using the VCSEL – 8 mA biasing). (a) Measured EVM curve comparing with each simulated EVM curve. (b) Measured and simulated EVM curves altogether.

B. Sharpness parameter effect on the model

Finally, we analyze the influence of the sharpness parameter on the link performance when the improved Cann's nonlinear model is used. To fully test the model, we perform AM/AM measurement for full frequency band and VCSEL bias current sweep, respectively from 1 to 6 GHz and from 4 to 10 mA. Then the Sharpness parameter is extracted through a mathematical fit of the experimental output power vs input power curves (AM/AM) over the range of the sweep parameters (frequency

and source current). The result for this Least Absolute Error (LAE) extraction provides the extracted k under the improved Cann's model as shown in figure 6.

At low VCSEL bias current, the sharpness parameter k values are lower. In this case, the operation point is very close to the threshold of the VCSEL, and this might be the cause of the nonlinearities. For higher biasing, the k parameter increases with respect to the frequency, which means that the curve becomes sharper. Hence, the transition between the linear and the saturation regions is faster.

The variation of the sharpness parameter can be explained by the change in the intrinsic dynamic behavior of the VCSEL as a function of the current bias. Figure 7 depicts the experimental result of P_{1dB} compression point of the VCSEL as a function of bias current and frequency. As the bias current of the VCSEL increases the relaxation oscillation frequency is also increased. This influences the nonlinearities of the VCSEL such as the P_{1dB} compression point also.

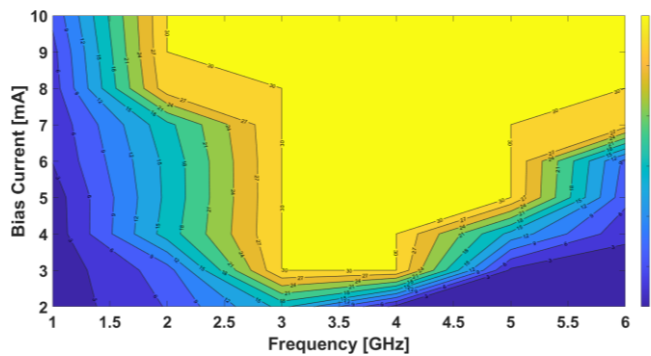


Fig. 6. Sharpness parameter as a function of the bias Current and the Frequency for improved Cann's model.

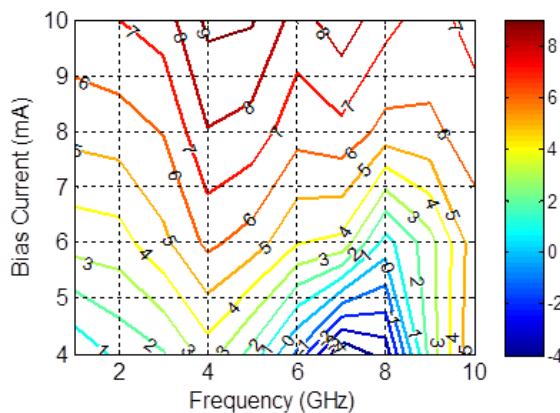


Fig. 7. The IP_{1dB} compression point (in dBm) of the VCSEL as a function of biasing current function of frequency.

V. CONCLUSION

This paper has proposed a behavioral model for VCSEL lasers employed into RoF systems with a focus on the modeling of their non-linearity. It exploits a Cann and Improved-Cann model, which were known previously in the field of RF power amplifiers and transposed in this paper to the opto-microwave domain. The resulting model includes the frequency response, RIN modeling and non-linear behavior.

Comparisons between the numerical simulations and measurements of the AM/AM curves over the range 1-10GHz and EVM data in the case of an LTE signal at 2GHz were provided for a VCSEL RoF link. The non-linearity sharpness parameter k is key to represent the non-linearity of the device. Its extraction over the full 1-6GHz has been provided showing that the parameter is highly dependent on the frequency and biasing current.

Behavioral modeling is in this regard an important approach that helps to provide a simple analysis of the component behavior into a system, or vice-versa to determine what are the minimum requirements in terms of compression point, non-linearity sharpness, bandwidth or gain for the device to operate into a given system.

While previous *tanh* model did not evaluate properly the region of EVM non-linearity, the proposed model provides a convenient tool that helps to predict the maximum k value for a device to operate with a given maximum EVM for example. It helps the selection of a given VCSEL of the prediction of the performance of a given laser into an overall system.

To improve the Cann's nonlinear model, and as further work, we are focusing on providing analytical expressions of some OM figures of merit. We are more particularly interested on the 1dB compression point and the third order intermodulation product. These parameters would depend on the saturation value and the sharpness variable.

ACKNOWLEDGMENT

This work was partly supported by the French FUI8 ORIGIN project and FUI MORF project and by the Université Franco Italienne - Università Italo Francese, through the sponsorship of the Joint Doctorate Project C3-2025 Efficient Wireless Coverage of In-Building Environments with Low Electromagnetic Impact within the Call Vinci 2019.

REFERENCES

- [1] A. Stohr et al "60 GHz radio-over-fiber technologies for broadband wireless services", Journal of optical communication and networking, May 2009.
- [2] B. Charbonnier et al "Photonics for broadband radio communications at 60 GHz in access and home networks" in International Topical Meeting on Microwave Photonics (IEEE, 2008), pp. 5-8.
- [3] M. Huchard et al "Ultrabroadband wireless home network based on 60-GHz WPAN cells interconnected via RoF," J. Lightwave Technol. **26**, 2364-2372 (2008).
- [4] A. Ng'oma, M. Sauer "Radio-over-fiber technologies for high data rates wireless applications" IEEE, 2009.
- [5] A. Ng'oma, G-J. Rijkenberg, A.M.J. Koonen "Building extended-reach radio-over-fiber links by exploiting optical frequency multiplication's dispersion tolerance" in Proc. Internat. Microwave Symposium, Honolulu, 2007, pp. 2179-2200.
- [6] C. Viana, Z. Gedeb Tegegne, J-L. Polleux and C. Algani, "Flexible new opto-microwave design approach for Radio-over-fiber applications: a case study of low cost 60 GHz VCSEL-based IF-RoF link" IEEE Transactions on Microwave Theory and Techniques Vol. 66, No. 9, Sept. 2018.
- [7] P. V. Mena, Sung-Mo Kang and T. A. DeTemple, "Rate-equation-based laser models with a single solution regime," in Journal of Lightwave Technology, vol. 15, no. 4, pp. 717-730, April 1997, doi: 10.1109/50.566695.

- [8] M.U. Hadi, J. Nanni, O. Venard, G. Baudoin, J.L. Polleux, G. Tartarini, "Practically feasible closed-loop Digital Predistortion for VCSEL-MMF-based Radio-over-Fiber links", in *Radioengineering Journal*, Czech and Slovak Technical Universities, 2020, 29 (1), pp.37-43
- [9] M.U. Hadi, C. Kantana, P.A. Traverso, G. Tartarini, O. Venard, G. Baudoin and J.L. Polleux, "Assessment of Digital Predistortion Methods for DFB-SSMF-Radio-over-Fiber Links Linearization", in the *Microwave and Optical Technology Letters*, July 2019
- [10] C. H. Cox III., G. E. Betts, and L. M. Johnson, "An analytic and experimental comparison of direct and external modulation in analog fiber-optic links", *MTT*, Volume 38, Issue 5, pp. 501–509, 1990
- [11] C.H. Cox, "Gain and noise figure in analogue fiber-optic links", *IEEE Proceedings Journal Optoelectronics*, Volume 139, Issue: 4, 1992
- [12] C.H. Cox, E.I. Ackerman, G.E. Betts, "Relationship between gain and noise figure of an optical analog link", *IEEE MTT-S International Microwave Symposium Digest*, Volume 3, 1996
- [13] C. H. Cox III, E. I. Ackerman, G. E. Betts, J. L. Prince, "Techniques and Performance of Intensity- Modulation Direct-Detection Analog Optical Links", *IEEE Transactions on Microwave Theory and Techniques*, Volume 45, No.8, pp. 1375-1383, 1997
- [14] E. I. Ackerman, C. H. Cox III, "State of the art in analog fiber-optic link technology", *ISSSE 98. 1998 URSI International Symposium on Signals, Systems and Electronics*, 1998
- [15] E.I Ackerman. C. Cox III, G. Betts, H. Roussell, F. O'Donnell, K. Ray, "Input impedance conditions for minimizing the noise figure of an analog optical link", *IEEE Transactions on Microwave Theory and Techniques*, Volume 46, Issue 12, 1998
- [16] E. I. Ackerman, "The effective gains and noise figures of individual components in an analog photonic link", *International Topical Meeting on Microwave Photonics*, Budapest, pp. 369-372, 2003
- [17] C. H. Cox III, E. I. Ackerman, G. E. Betts, J. L. Prince, "Limits on the Performance of RF-Over-Fiber Links and Their Impact on Device design", *IEEE Transactions on Microwave Theory and Techniques*, Volume 54, No.2, pp. 906-920, 2006
- [18] E.I. Ackerman, W.K. Burns, G. Betts, J.X. Chen, J.L. Prince, M.D. Regan, H.V. Roussell, C.H. Cox III, "RF-over-fiber links with very low noise figure", *Journal of Lightwave Technology*, Volume 26, No; 15, 2008.
- [19] H.A. Haus, "Noise Figure Definition Valid From RF to Optical Frequencies, *IEEE Journal Selected Topics in Quantum Electronics*, Volume 6, pp.240-247, 2000.
- [20] D.M. Baney, P. Gallion, R.S. Tucker, "Theory and Measurement techniques for the noise figure of optical amplifiers", *Optical fibre Technology* 6, 122-154, 2000, pp.122-154.
- [21] R.S. Tucker, D.M. Baney, "Optical Noise Figure: Theory and Measurements", *Optical Fiber Communication Conference*, Volume 3, pp. W11-1-3, 2001.
- [22] I. Frigyes, B.G. Habermajaer, A. Molnar, A. Seeds, F. Som, "Noise and loss characteristics of microwave direct modulated optical links", *27th European Microwave Conference*, Volume 1, 1997
- [23] G. Plantier, C. Bes, T. Bosch "Behavioral model of a self-mixing laser diode sensor", *IEEE Journal of quantum electronics*, vol 41, issue 9, Sept 2015.
- [24] A. Gameiro, N. J. Gomes, P. P. Monteiro "Next Generation Wireless Communications using Radio over Fiber" chapter 10, section 3, 2012.
- [25] Kai-Lun Chi et al "Single-mode 850nm VCSELs for 54 Gbit/sec On-Off Keying Transmission over 1km Multi-Mode Fiber" *IEEE Photonics Technology Letters*, 28:1-1, June 2016.
- [26] J. Estaran et al "Quad 14 Gbps L-band VCSEL-based system for WDM migration of 4-lanes 56 Gbps optical data links" *Optics Express* 20:28524-31, Dec. 2012.
- [27] Crespo-Cadenas, C., J. Reina-Tosina, and M. J. Madero-Ayora, "Volterra behavioral model for wideband RF amplifiers," *IEEE Transactions on Microwave Theory and Techniques*, Vol. 55, 449–457, 2007.
- [28] Zhu, A. and T. J. Brazil, "Behavioral modeling of RF power amplifiers based on pruned volterra series," *IEEE Microwave and Wireless Components Letters*, Vol. 14, 563–565, 2004.
- [29] Mirri, D., G. Luculano, F. Filicori, G. Pasini, G. Vannini, and G. P. Gabriella, "A modified Volterra series approach for nonlinear dynamic systems modeling," *IEEE Transactions on Circuits and Systems I: Fundamental Theory and Applications*, Vol. 49, 1118–1128, 2002.
- [30] Zhu, A., J. C. Pedro, and T. J. Brazil, "Dynamic deviation reduction-based volterra behavioural modeling of RF power amplifiers," *IEEE Transactions on Microwave Theory and Techniques*, Vol. 54, 4323–4332, 2006.
- [31] Isaksson, M. and D. Ronnow, "A kautz-volterra behavioral model for RF power amplifiers," *IEEE MTT-S International Microwave Symposium Digest*, 485–488, 2006.
- [32] Zhu, A. and T. J. Brazil, "RF power amplifier behavioral modeling using Volterra expansion with Laguerre functions," *2005 IEEE MTT-S International Microwave Symposium Digest*, 963–966, 2005.
- [33] Hyunchul, K., M. D. McKinley, and J. S. Kenney, "Extraction of accurate behavioral models for power amplifiers with memory effects using two-tone measurements," *2002 IEEE MTT-S International Microwave Symposium Digest*, 139–142, 2002.
- [34] Cabral, P. M., J. Pedro, and N. B. Carvalho, "Modeling nonlinear memory effects on the AM/AM, AM/PM and two-tone IMD in microwave PA circuits," *International Journal of RF and Microwave Computer-Aided Engineering*, Vol. 16, 13–23, 2006.
- [35] Hui Wang, Peiguo Liu "Behaviorals Models for Power Amplifiers using a Difference-frequency Dual-signal Injection Method" *PIERS Proceedings*, March 2010.
- [36] A. J. Cann, "Nonlinearity model with variable knee sharpness," *IEEE Trans. Aerosp. Electron. Syst.*, vol. AES-16, pp. 874–877, Nov. 1980.
- [37] CaA. J. Cann, "Improved Nonlinearity model with variable knee sharpness," *IEEE Trans. Aerosp. Electron. Syst.*, vol. 48, no.4, pp. 3637–3646, March 2012.
- [38] Loyka S. "On the use of Cann's model for nonlinear behavioral-level simulation". *IEEE Trans. on Vehicular Technology*, 49, 5, Sept. 2000.
- [39] C. J. O'Brien, M. L. Majewski, A. D. Rakic, "A critical comparison of high-speed VCSEL characterization techniques", *Journal of Lightwave Technology*, Volume 25, Issue 2, 2007